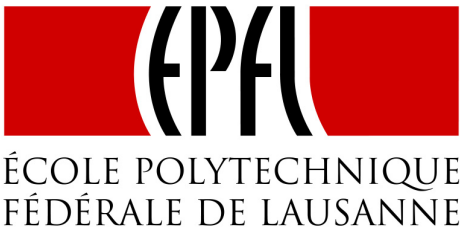

Semester Project Report

Bio-inspired Methodology for Sprawling Posture Robotic Foot Design

Author:
Laura Paez

Supervisors:
Kamilo Melo
Robin Thandiackal

Professor:
Auke Jan Ijspeert

June 8, 2015

Contents

Executive Summary

The design of a foot for a sprawling posture animal may vary as there are significant differences between biological species. A systematic search inside the taxonomy of different species, led to identify some representative organisms, some of them with related biomechanic literature, that serves as a basis to identify some differences as well as common characteristics across species. The outcome of this analysis, was a map that classifies some species, and groups them in clusters with similar biomechanic characteristics as speed, body mass, body length. This was important as is provided with some insights of how to look at the skeletal structure across species, to define important characteristics for the design of a robotic foot.

The next step, was the design of a generic foot, in which the dimensions, angles, aspect ratios and the kinematics of different species in general was condensed in simple parameters. A contribution so far was on the classification of morphologies and the extraction of simple parameters that allow the design of different feet for different sprawling animals. This previous analysis was implemented physically by modifying the compliant hand design of Pisa/IIT to match the expectations and design parameters of one selected organism, the Tiger salamander (Ambystoma tigrinum) foot. We chose this species, for two reasons, first because there is abundant literature on the skeletal structure of this animal, and second, because the implementation can be easily ported to robots like Pleurobot. Then, We scaled up the dimensions of the organism foot, according to the kinematics of the experimental setup used to test the foot.

A set of experiments were carried out using the MoCap to retrieve the kinematics of the foot and the force plates, in order to compare with the results, especially ground reaction forces (GRF), with the literature. The experimental setup built for this purpose, consisted in a simulated planar robotic leg with a rail that allow the horizontal displacement of the body while maintaining the foot static with the force plate. Vertical motion was constrained which affects the GRF, but still allowing an interesting visualization of the behavior of the normal forces along the whole standing phase.

The results of this project were merely quantified to validate the design and to provide a tool for the lab for both, design generic feet as well as to examine their behavior prior implement it in a real robot. For this reason, there is still a lot of work to be done on this area. In the biological classification and extraction of features for foot design as well as their implementation and validation. Nevertheless, We hope this report and all the interesting contributions on it will create a useful precedent for future work in the EPFL's Biorobotics Lab.

Chapter 1

Introduction

The experience gained in the Biorobotics Laboratory at EPFL with several implementations of salamander robots through the last years (Amphibot [1], Salamandra robotica [2], Pleurobot, etc), open new avenues for the study of robotic devices that complement the current state of this technology. In particular, the use of Pleurobot (a 27 degree of freedom salamander robot with rich motions on spine and limbs designed from a real organism) as platform to test neuromotor hypothesis serve as basis to identify some hardware needs that enrich the current locomotion experiments and hopefully serve as answer for some hypotheses related to an interesting newly discovered gait, the aquatic stepping.

The hypothesis are based on the fact that aquatic stepping gaits present a higher speed performance as well as efficiency (i.e. lower cost of transport) compared to other gaits using the limbs (i.e walking). This suggest that the foot structure and function contributes at a great extent on the propulsive force generation. From biological observations (i.e. videos of living giant salamanders), as well as literature associated to sprawling posture animals (that will be cited along the report), the feet contribute to the body thrust in the sense that they increase the standing phase part of the stride cycle (i.e. with the finger contact), while keeping the limb kinematics reduced, thus expending less energy. In the same way, the compliant characteristic of the fingers while in contact with the ground, add a passive mechanism to maintain traction and produce extra thrust every stride. In other words, this hypothesis can be stated as: *Fingers and the whole foot structure are important for walking gaits in sprawling posture robots, especially for aquatic stepping gaits, as some recent experiments using Pleurobot indicate a thrust generation due to the finger push off the ground.*

This hypothesis, if it holds true, provides a significant contribution to the underlying mechanisms of the locomotion of salamanders and other sprawling posture animals, complementing the current body of knowledge. This is a sufficient justification for the exploration of a robotic foot, whose design is directly inspired from biology both in its form and function.

Chapter 2

Design Methodology

This is the first of the main sections of this report. In here, a bio-inspired design methodology of a robotic foot is proposed. It starts with a systematic search in animal taxonomy to find relevant species that present characteristics like sprawling posture and undulating spine. Then, a section that explain how these relevant species can be grouped in clusters for given biomechanical characteristics lead the way to the extraction of specific foot design parameters.

2.1 Systematic selection of representative species

The main purpose of this project is to provide a tool that complements the current robot technology available to test scientific hypotheses. In particular, the current robots are inspired in the morphology of salamanders and other amphibious animals. Taking this as starting point, salamanders are characterized, among other species, by its sprawling posture and the undulatory lateral movement on its spinal cord, while they walk. Keeping these two aspects in mind, We decided to evaluate using a systematic search across the animal taxonomy, looking for different organisms that present these two characteristics. The search consisted in look inside the animal taxonomy, identifying in a Top-Down approach different paths in taxonomy that lead to representative organisms that feature the two aforementioned characteristics.

Trying to be as general as possible, the search started with the kingdom *Animalia*. In the level below, one can identify the phylums *Chordata* and *Arthropoda* as the only ones that present species with sprawling posture. However, *Arthropoda* was rejected as the organisms that conform this phylum do not have a spinal cord with undulatory movement. Inside *Chordata*, there are organisms with backbones (i.e. subphylum *vertebrata*) where the superclass *Tetrapoda* has place. *Tetrapoda* has two classes that match the desired features. There are: *Reptilia* and *Amphibia*. As part of the *Reptilia* class, turtles are discarded as they have a sprawling posture, however no lateral undulation in the spinal cord is present. On the other hand, *Crocodilia* and *Squamata* are two orders inside *Reptilia*, that match the desired features with more than one living species. *Crocodilia* has the crocodiles and the alligators. The species *Osteolaemus tetraspis* and *Alligator mississippiensis* are taken into account as representatives of *Crocodilia* order. The *Squamata* order contains the snakes and lizards, but as the snakes are limbless, only lizards are taken into account (i.e. *Lacertelia* sub-order). Six different species were selected inside *Lacertelia* sub-order. Different lizards with varying speeds and size are considered. Lizards with climb capabilities like genus *Gekko*, were not considered, as the priority is not on climbing animals. The chosen species

were: *Uma scoparia*, *Phrynosoma platyrhinos*, *Callisaurus draconoides*, *Dipsosaurus dorsalis*, *Cnemidophorus tigris* and *Varanus panoptes*.

The *Amphibia* class contains frogs, who have a sprawling posture but they lack an undulatory spinal cord. In the same way, there are limbless animals or animals with just two limbs, which are not considered. The order *Caudata*, on the other hand, contains the salamander species, and includes the selected sub-orders: *Cryptobranchoidea* and *Salamandroidea*. The Giant salamander belongs to the *Cryptobranchoidea* sub-order. The species *Andrias japonicus* was chosen as a representative of this order. Three different species belonging to three different genus, from *Salamandroidea* were selected as: *Dicamptodon tenebrosus*, *Pleurodeles waltl* and *Ambystoma tigrinum*.

The search in animal taxonomy was not straightforward, as it demanded a thorough literature review on several species, particularly the species which are reported concerning animal locomotion. Summarizing, the systematic search results in a tree shape that can be seen in Fig. 2.1. The biomechanical parameters that correspond to each species are reported in table 2.1 as well as the relevant literature employed.

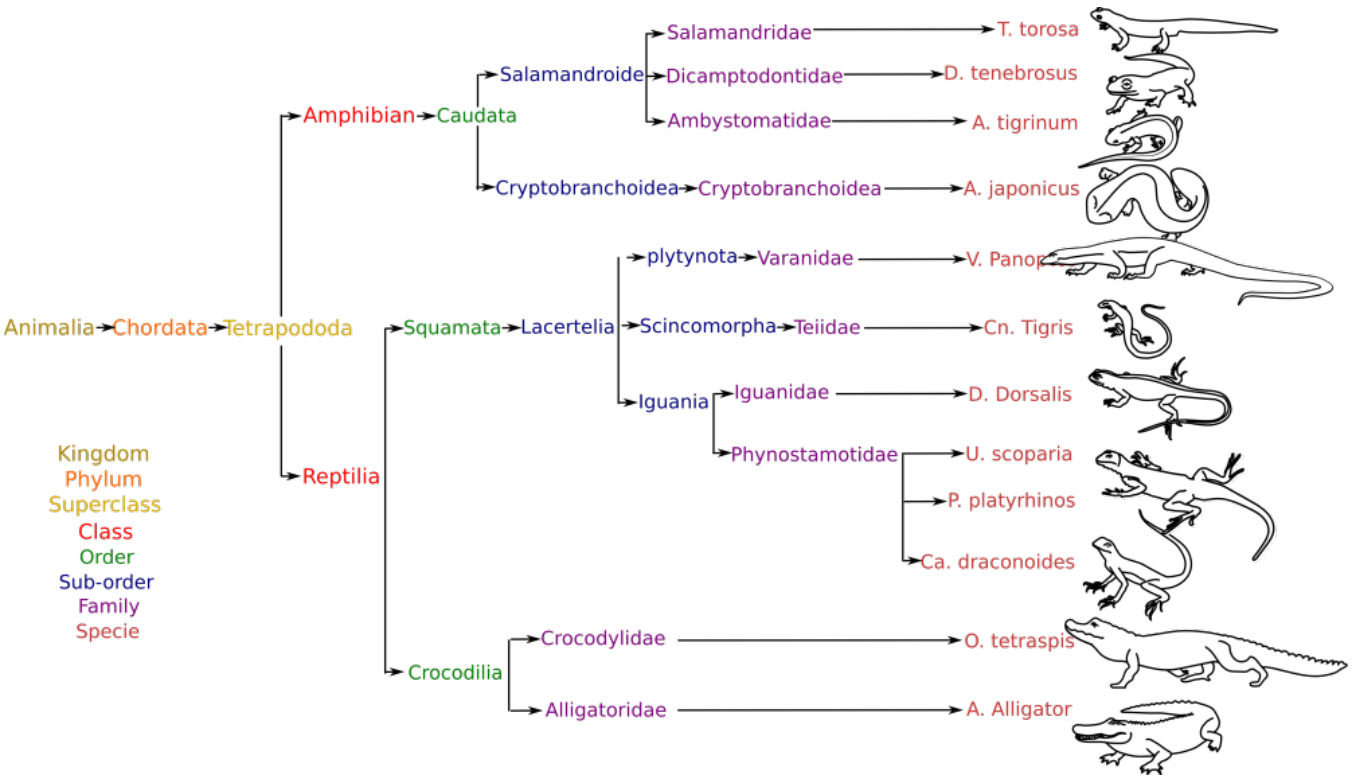

Figure 2.1: Systematic search results, showing selected species.

2.2 Clustering of species by biomechanic evaluation

The design methodology presented in this report, has as main objective the definition of guidelines for the implementation of a robotic device. Biological classification of sprawling posture animals described in the previous section provide a reduced set of species for analyze. However, the

biomechanic characteristics of the selected species still differ one from each other at a great extent. The purpose of this section is to re-classify by grouping (clustering) the selected representative species according to the biomechanic parameters: speed of locomotion, body mass and body length (i.e. snout-to-vent length), in order to identify common features shared by different species. These biomechanic parameters, are interesting as any robot can be compared with any animal species using the same metrics. In biorobotics most of the robots implemented are scaled copies of real organisms (or part of their bodies). The biomechanic parameters used here can be easily scaled or the impact of their scale can be predicted by scaling laws, making this analysis convenient for a design bio-inspired.

A search across the literature was done, in order to find the selected parameters in the species mentioned above. Table 2.1 summarizes the information found in the literature with its respective reference. For some species, an overlap of information from literature was present, which was averaged; for other species, finding relevant literature with reliable data was difficult. In this case, either a different (close in taxonomy) species was selected from the same genus or information was extracted from animal encyclopedias.

	A. mississippiensis	**O. tetraspis**	**U. scoparia**	**P. platyrhinos**
Speed (m/s)	6.667	4.722	3.8-4.1	2.0-2.2
Mass (g)	(181-363)x10^3	(18-32)x10^3	20.22-13.78	23.03-28.37
Length (m)	0.025- 4.5	1.7 - 1.9	0.074-0.086	0.078-0.079
Source	[3]	[4]	[5]	[5]
	C. draconoides	**D. dorsalis**	**Cn. tigris**	**V. panoptes**
Speed (m/s)	4.1-4.3	3.6-3.7	3.15-3.25	6.3
Mass (g)	8.0-11.0	22.35-25.65	16.3-18.3	1243
Length (m)	0.071-0.081	0.083-0.091	0.085-0.086	0.041
Source	[5]	[5] [6]	[5]	[7]
	A. japonicus	**D. tenebrosus**	**P. waltl**	**A. tigrinum**
Speed (m/s)	0.32	0.062-0.279	0.053	4.722
Mass (g)	(25-30)x10^3	14-42	50-100	113-227
Length (m)	1-1.5	0.081 0.096	0.085-0.1	0.015-0.035
Source	[8]	[9] [10]	[11]	[12]

Table 2.1: Parameters of selected species

With the biomechanic information extracted (Table 2.1), a 3D-biomechanical map as is shown in Fig. 2.2 was made. This allows to find how different species can be grouped in clusters. Parameters like body mass, has values that span between 363000 and 8 grams (i.e. *A. Alligator* weights up to 363000 grams and *C. Draconoides* could weight 8 grams). As the scale needed to cover these boundary values, a logarithm scale is applied. Likewise, a logarithm scale is applied to body mass, which also presents widely spanned values. Fig. 2.2b and Fig. 2.2c show the 2D views of Fig. 2.2a to improve the readability of the information.

The purpose of these plots is twofold. At first, for from-scratch-robot-design purposes, the robot designer can locate him/herself into the plot and learn how the different biomechanical parameters (speed, body mass and body length) combine in respective clusters of species. This is a way to select one correct combination of expected design parameters as nature has been optimizing such parameters by evolution. For example, if the designer expects a fast robot, he/she can notice that these high speeds are also constrained by certain amounts of body mass

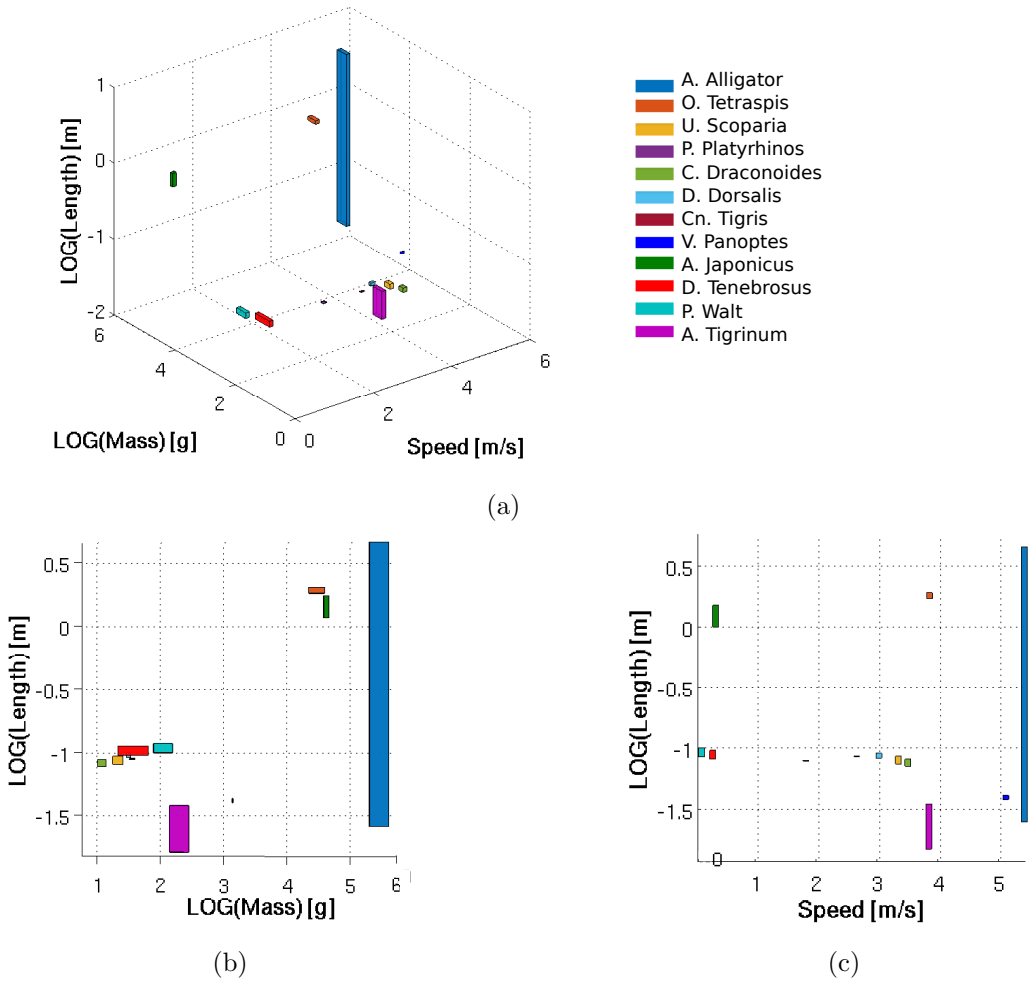

Figure 2.2: Parameters of selected species, in (a) 3D, in (b) Length vs Mass, in (c) Length vs Speed

and length in the plot. Then, with the respective scaling by choosing one or two initial design parameters, the others are suggested by the plot in order to have an optimal-by-nature solution. This is the essence of the bioinspired design methodology.

The second purpose of the clustering, is less general but more focused in the main contribution of this project. If the robot designers have already a robot (e.g. Pleurobot) with certain biomechanical characteristics, but they want to design a certain part of the functional body of the animal (i.e. limbs, foot, tail). The designers then, can locate it in the plot (i.e. locate the current speed, body length and mass) and analyze which organisms share similar features (of course taking into account the scale). This allows the selection of an animal or animals within the cluster, that fit with the needs and the existing robot features to extract the specific body part design information. For instance, the skeletal information of an animal's foot that matches the expected speed ranges of a robot, the max-min animal kinematic parameters (i.e. angles) for the motion of robot limbs, the musculo-skeletal information (i.e. tendon elasticity, peak forces) for design of compliant legs, and so on.

2.3 Foot design parameters

Taking into account the classification by clustering previously done, a new search were done. It consisted in look for skeletal information of foot bones, of each species chosen. However, the new investigation span the families (i.e. not just the selected species, also other species belonging to the same family), in order to include more fruitful data. This is valid as most of the family species members employed fall into the same cluster of biomechanical characteristics. The selected information, mostly photos, schematic drawings, X-ray pictures, diaphonized bones and foot bone length data, were found from different and variety sources: journal papers, museum photographic databases, and so on [13–33]. Fig. 2.3 shows some examples of the figures used into this analysis, it includes pictures of alligator, salamander and lizard feet.

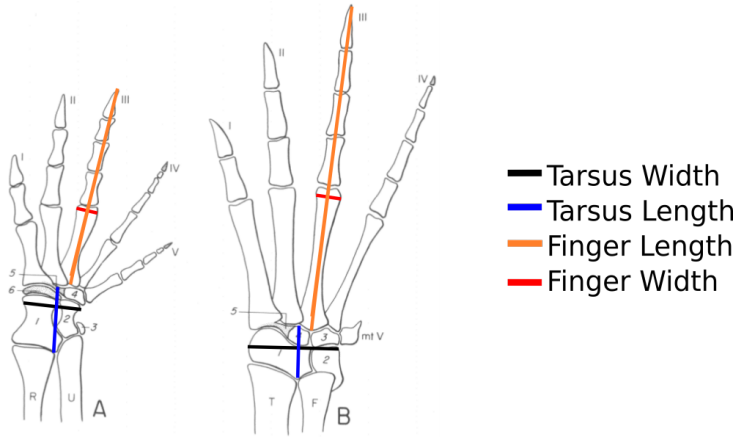

(a)

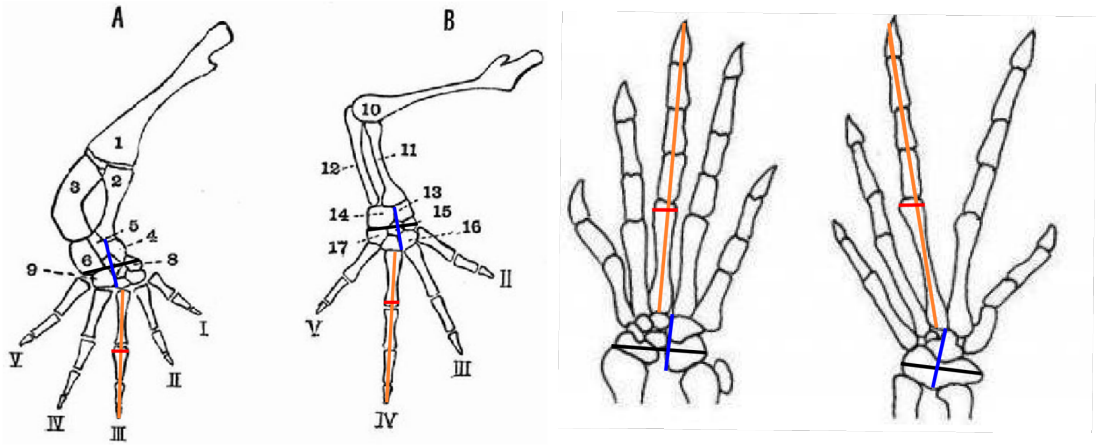

(b)

(c)

Figure 2.3: Details of length measures taken from images are shown. (a) Alligator feet [16]: forelimb (left), hindlimb (right). (b) Salamander feet [15]: forelimb (left), hindlimb (right). (c) Lizard feet [14]: forelimb (left), hindlimb (right).

Using the information mentioned above, four measures were considered: the tarsus width, the tarsus length, the longest finger length and finger width. This selected measures captured the general length features of any foot as observed across this study. Fig. 2.3 shows examples

of how these measures were taken. As the measures come from different sources, with different sizes (but with same relation between measures due to species from the same family) a data normalization was carried out, taking the finger width as a reference measure, because it is the smallest measure[1]. The other parameters (i.e. tarsus width, tarsus length and finger length) were divided by the finger width value. As a result all the parameters are in function of the finger width. Finally, the average inside the species' family data is done, and the final results can be seen in Table 2.2.

ForeLimb					
Animal	**Family**	**Tarsus Width**	**Tarsus Length**	**Finger Length**	**Finger Width**
Lizard	Phrynosomatidae	5.07	3.67	9.54	1.00
	Iguanidae	3.66	3.03	13.39	1.00
	Scincomorpha (subOrder)	3.45	2.72	8.70	1.00
	Varanidae	3.21	1.67	6.61	1.00
Salamander	Cryptobranchoidea	3.52	1.97	3.37	1.00
	Dicamptodontidae	3.15	2.45	7.55	1.00
	Salamandridae	3.97	3.56	11.20	1.00
	Ambystomatidae	3.02	2.80	6.02	1.00
Alligator & Crocodile	Alligatoridae	2.81	2.98	9.11	1.00
	Crocodylidae	4.02	4.29	14.65	1.00
HindLimb					
Animal	**Family**	**Tarsus Width**	**Tarsus Length**	**Finger Length**	**Finger Width**
Lizard	Phrynosomatidae	4.40	3.01	18.56	1.00
	Iguanidae	4.17	3.78	21.16	1.00
	Scincomorpha (subOrder)	4.29	2.43	16.56	1.00
	Varanidae	5.17	3.00	8.41	1.00
Salamander	Cryptobranchoidea	3.02	2.12	5.24	1.00
	Dicamptodontidae	3.81	3.45	9.08	1.00
	Salamandridae	4.30	4.48	11.70	1.00
	Ambystomatidae	4.90	4.76	8.74	1.00
Alligator & Crocodile	Alligatoridae	4.88	3.56	17.81	1.00
	Crocodylidae	5.14	2.16	18.38	1.00

Table 2.2: Mechanical design parameters extracted from diiferent species hind and fore limb's feet.

[1] In a robot design, this might be the most important parameter as is directly related with the miniaturization capabilities of the mechanical structure i.e. minimum mechanical parts resolution.

Chapter 3

Implementation

Following the guidelines for organism selection based on biomechanic parameters described before, in this chapter a robotic implementation of a foot is presented. First of all, an animal species is selected according to information available on literature, in order to replicate its foot, followed by the definition of some kinematic and mechanical features specific to the selected species that will constrain the final implementation. Then, the technology selection is introduced and the mechanical design of the robotic foot is explained in detail. At the end of this chapter, a comparison between the final foot implementation and the expected dimensions coming out from the biomechanical analysis are presented and discussed.

3.1 Animal species and features design selection

The main objective of the implementation example of a foot design that will be shown in this report, is to validate the design methodology mentioned before. For this reason, in order to present the best validation possible, one can look for a species with more biomechanic literature available. The Tiger salamander (*Ambystoma tigrinum*) was selected. Among all the information presented in [34], including bone structure and bone dimensions, it is possible to find important data related to the kinematics of the stride and, very important measurements of ground reaction forces (GRF). These GRFs will be very important to compare with experimental measurements, that the robotic foot implementation complies with the natural behaviors of real animals.

Design parameters for the hind right foot were chosen, as hindlimbs provide most of the thrust during the walking gait [35]. In [33], M. Ashely-Ross provides information about muscles and bones for Tiger salamander hindlimbs. The hind feet, in most of the species including the aforementioned one, are characterized to be bigger than front feet, and have five toes. The longest finger has three phalanges and the shortest one only 2 (Fig. 2.3). Every finger has an orientation with respect to the adjacent one of approximately 20°, being normally the central finger aligned in a straight line with the crus. According with literature cited in previous semester projects at Biorob ([36], [37]) and in the work of Karakasiliotis [38], an angle between tibia and tarsus should be considered. Likewise, the angle between phalanges and metatarsus is important to be included in the design to closely match the expected kinematics. Fig. 3.1 shows the selected angles and locations of each one of the aforementioned angles.

A design decision was made at this point, which makes part of the methodology for the foot design. As mentioned in previous sections the finger width is important in the mechanical design

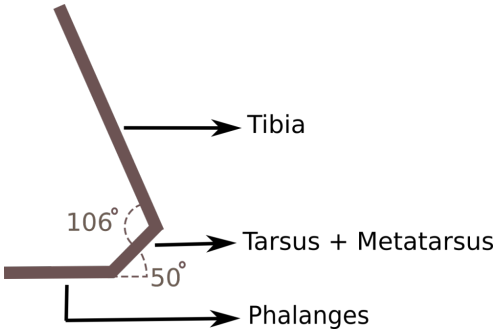

Figure 3.1: Limb schema in "home" position, showing the angles between phalanges and metatarsus, and between tarsus and tibia.

of the foot as they offer a limitation in the miniaturization of the mechanical parts. For this reason, the overall size of a complete foot realization is also limited. Moreover, sprawling posture animals do not use their fingers for specialized tasks like manipulation. Moreover, the purpose of this project attempts only to the use of feet for locomotion purposes. In this order of ideas, reducing the number of fingers by fusing together two or more fingers in a single one, will maintain the overall behavior expected in locomotion while allowing the reduction of design dimensions under the nominal values.

Consequently, in order to reduce the mechanical components in the final implementation (i.e. reducing materials, weight, size, etc.), and taking into account that side-most fingers in the selected species (*Ambystoma tigrinum*) are small in comparison to other fingers, three fingers were implemented in the current project. Two of them are large and the third one small. The large fingers attempt to represent this fusion of two fingers. Each of the large finger is composed by three phalanges, while the small one is composed by two.

3.2 Technology Selection

3.2.1 Hillberry Joint

The Hillberry joint [39], is a prosthetic joint initially used for knee joint purposes as it resembles a real biological inter-bone articulation. It consists of two cylinders that keep contact and are movable between each other, through the use of a flexible strap, that wraps them. As a result, a revolute joint, with a low joint friction, a wide rotation range and close to nature mechanism, can be obtained.

3.2.2 Mechanical parts

The Hillberry joint looks promising for its reduced complexity and high range. The University of Pisa and IIT, developed a robot hand prototype called Pisa/IIT SoftHand [40]. It is characterized by its robustness and the use of Hillbery joints as passive components that allow the introduction of compliant behaviors for their use in grasping. As the authors provide information related to the SoftHand as an open source hardware project, We decided to use it as a base for the proposed foot design in this project. In addition, the use of compliant mechanics in the design of a foot, matches the expected biomechanical behaviours of a real sprawling posture animal.

The design proposed here aims to validate the methodology described in the last chapter. Thus, it was necessary to design from scratch several parts using CAD tools like Solidworks and FreeCAD, and modify others taken from the open source hardware project mentioned before.

The Pisa/IIT SoftHand uses a wire across it that joins all the parts together and they are guided by means of small pulleys and bearings. It also has a single motor, that pulls the wire when actuated. Through the tension applied by this wire, the hand grasp (i.e. when the wire is pulled, the tension exerted increases and the hand closes the fingers). In this project, the wire is pulled by a single motor as well. However the design was made to modify both tension in the fingers during the last part of the stride (i.e. to increase thrust), as well as to bend the ankle/wrist in the desired kinematic trajectory during the swing phase. The analysis of when and how to actuate the finger and ankle joints was done by carefully checking X-ray videos (frame by frame) of animals like salamanders and lizards provided by Biorob and external literature.

3.2.3 Finger design

In order to generate the angles explained on Fig. 3.1 three initial finger prototypes were generated. Differences across these prototypes are in the location of the initial angle (i.e. home angle) of 50° between the metatarsus and the phalanges.

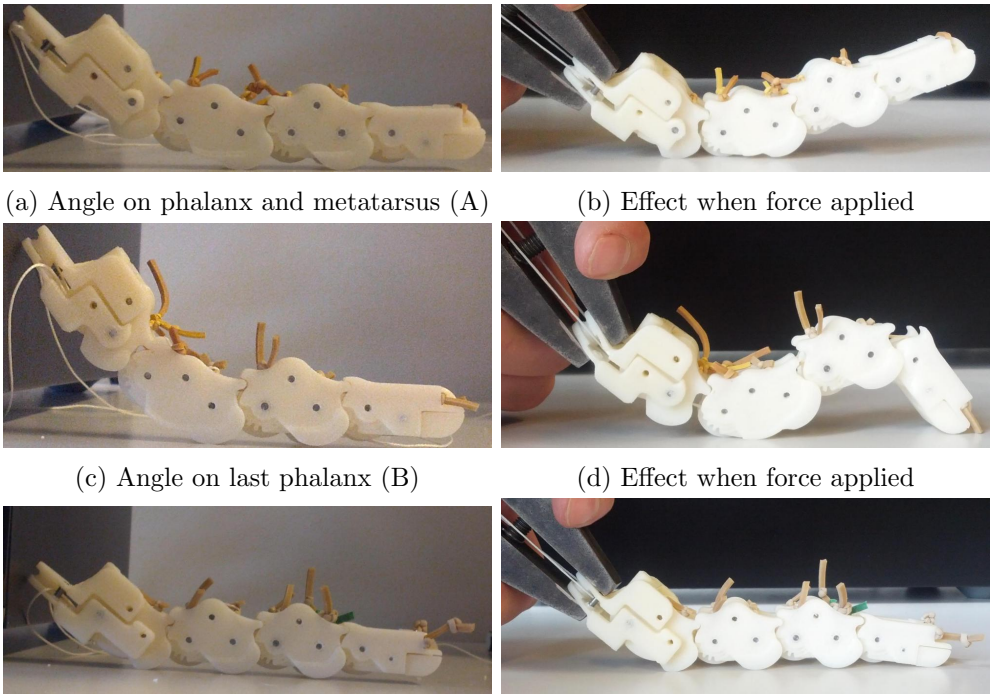

(a) Angle on phalanx and metatarsus (A) (b) Effect when force applied

(c) Angle on last phalanx (B) (d) Effect when force applied

(e) Angle on metatarsus (C) (f) Effect when force applied

Figure 3.2: Testing angle modifications effects

The first finger prototype (A), shown on Fig. 3.2a consisted in modifying the phalanx and the metatarsus parts by applying 25° on each of them. The second one (B) (Fig. 3.2c), consisted on modify the last phalanx by applying 50° only on it. Finally, the third one (C) has the 50° only on the metatarsus part, as shown in Fig. 3.2e.

Then, the selection of the best finger prototype, was made trough a force test. It consisted in pulling up the wire that drives the finger actuation (It makes the finger stiffer) and then applying a vertical force. This force simulates the weight of the robot that uses the foot. This makes it possible to identify the behavior of the finger once it is supporting the robot's weight. Fig. 3.1 right side, shows the effects generated onto the finger. By modifying the two pieces like shown in Fig. 3.2a (prototype A), the finger raise from the ground as shown on Fig. 3.2b. If the phalanx is modified (case on Fig. 3.2c) (prototype B), as a result the finger makes an arc as shown on Fig. 3.2d. Finally, if the desired angle is implemented on the metatarsus (as shown on Fig. 3.2e, prototype C) the finger stays in a straight position with all the phalanges keeping contact with the ground, as can be seen on Fig. 3.2f, regardless of the vertical force applied. These results show that the prototype (C) using only the metatarsus to provide the angle has the best performance. Hence, it was selected for the final implementation.

3.2.4 Mechanical integration

CAD files of the mechanical parts are available in the additional material, some of the parts can be seen on Fig. 3.3. Parts are made of ABS and manufactured by a 3D printer. The motor selected to drive the actuation of the whole foot is a Dynamixel MX-28R. The wire selected was Dyneema® of 0.5mm of diameter and 120kg of maximum tension. For the internal wire guidance (as seen in 3.3d, showing holes for the pulley rotational axes) several pulleys of different radii were used. Likewise to guide the wire inside the fingers, pulleys with bearings were used. The pulleys range from sizes of 6.2mm to 8mm in their external diameter, using miniature bearings of 4mm to 5mm external diameter with pin axes of 1.5mm to 2mm diameter. A total of 94 pulleys was used.

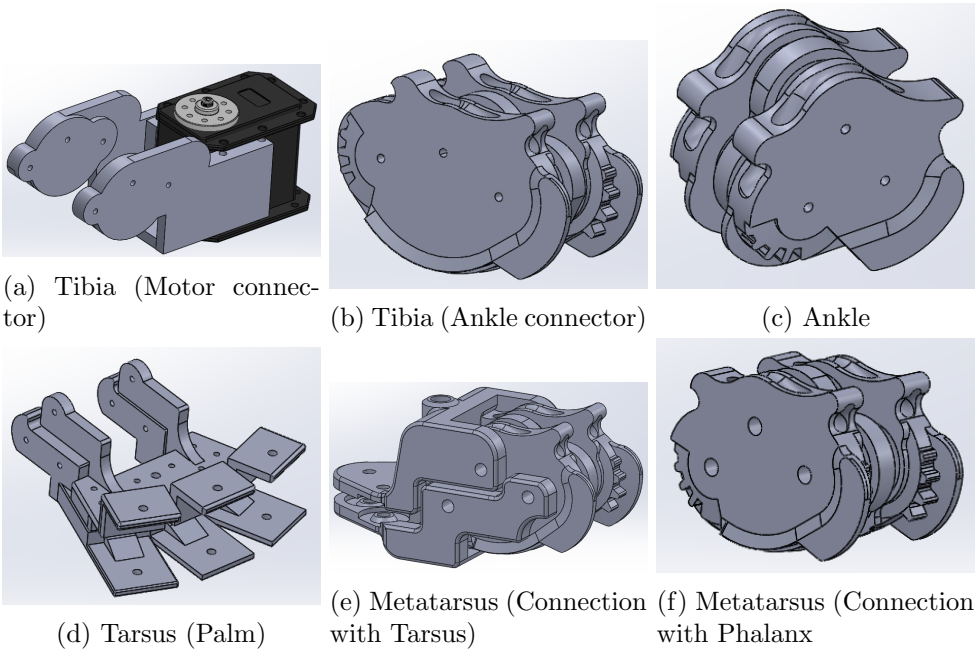

(a) Tibia (Motor connector)

(b) Tibia (Ankle connector)

(c) Ankle

(d) Tarsus (Palm)

(e) Metatarsus (Connection with Tarsus)

(f) Metatarsus (Connection with Phalanx

Figure 3.3: Mechanical parts

Fig. 3.3a represents part of the tibia (crus), and is the connection with the motor. The part

in Fig. 3.3b, provides the 106° between the tarsus and the tibia (as described in Fig. 3.1). The part in Fig. 3.3d is the tarsus, and it has the connection with the metatarsus part (i.e. Fig. 3.3e) from one side, and the other side has the part shown in Fig. 3.3c. Finally, the part shown in Fig. 3.3f provides the 50° between the fingers and the metatarsus.

The final assembly of the whole foot can be seen in Fig. 3.4. The right hindlimb was chosen, but the left one can be easily extracted by mirroring the different parts in Solidworks.

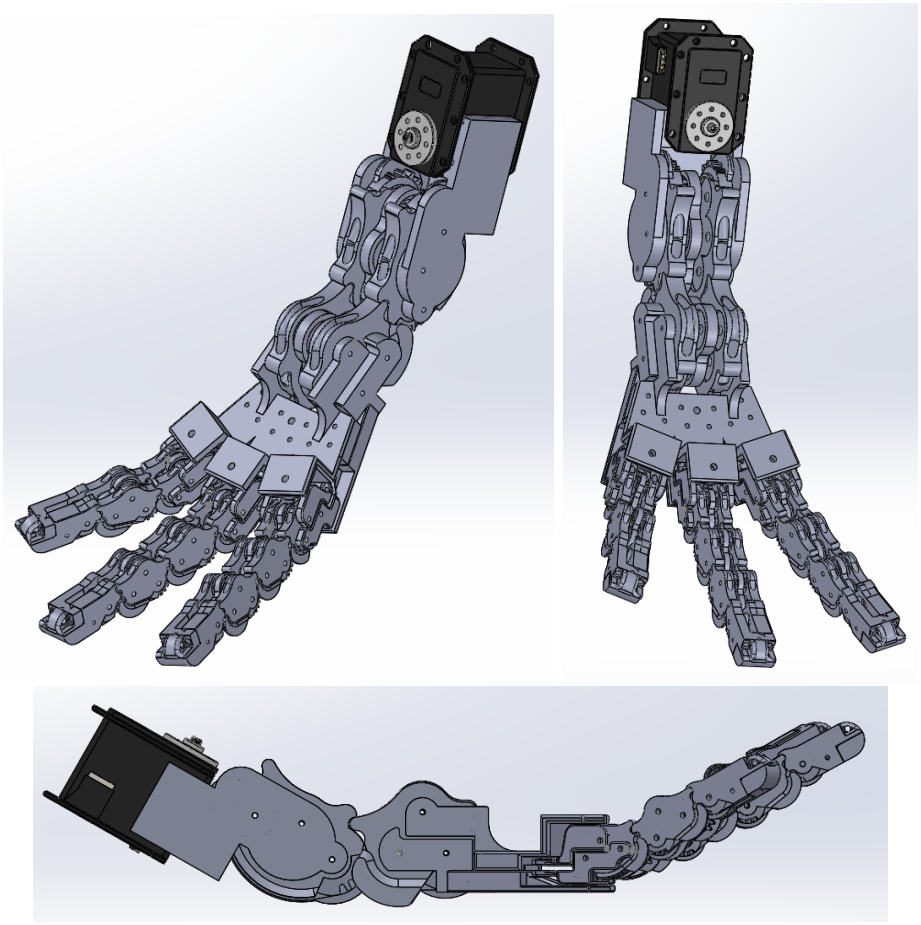

Figure 3.4: Final Foot Design.

Additionally, elastic rope was used to connect all the parts. This rope made part of the design specification. Selected values of elasticity were tested to find an appropriate one. The selection of the rope was made in order to provide a desired compliant behavior in the foot with expected loads comparable with a robot like Pleurobot. In the case of this design, 5mm diameter rope was used in the ankle and 2mm diameter rope was used in the fingers like seen in Fig. 3.5 on top.

Finally, an industrial high grip glove was modified by removing fingers and sewing the holes to match the dimensions of the foot. This glove, provided enough grip in the contact surface with the ground to prevent the foot to slip during experiments as seen in Fig.3.5 in the bottom row.

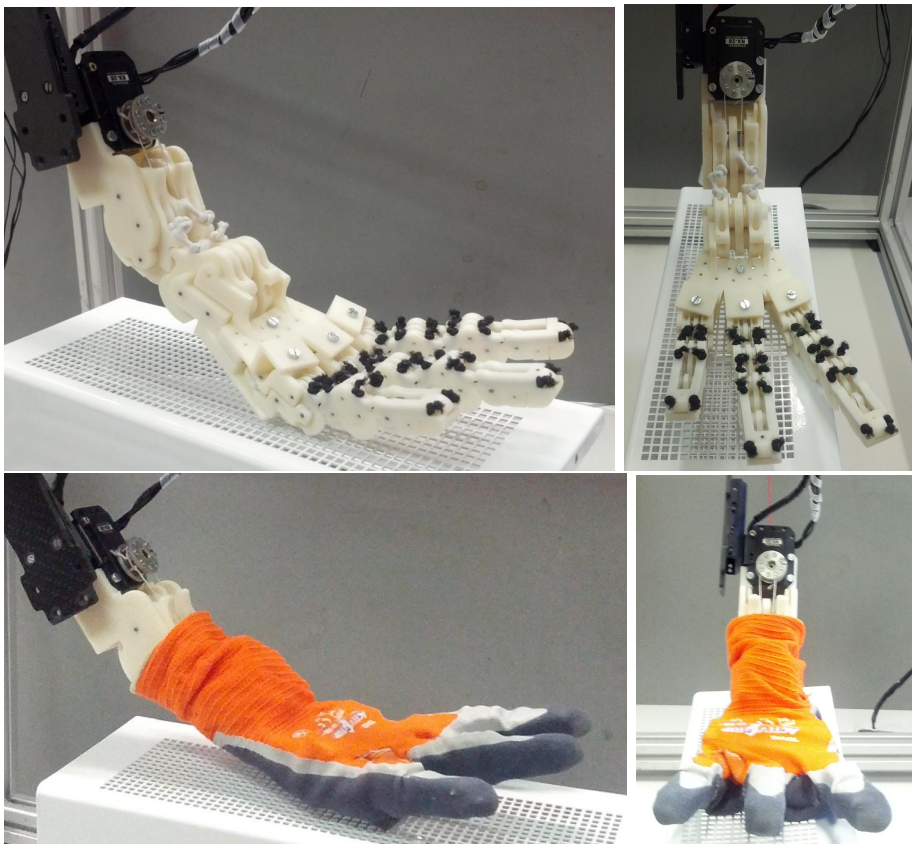

Figure 3.5: Foot implemented

3.3 Animal vs Robotic Foot

There were differences between the final design and the foot characteristics (i.e. representative organism foot lengths) that inspired such a design. Table 3.1 quantifies these differences, showing the error between them. As it is possible to observe, the errors are small in the case of the tarsus width fulfilling the expected dimensions. For the tarsus and finger length, the implemented dimensions exceed the nominal values in an almost 18% and 10%. However, their impact in the overall kinematics and final behavior is negligible. Further adjustments can be done in further versions by simply changing parameters in the CAD files.

	Tarsus Width	Tarsus Length	Finger Length	Finger Width
Normalized parameters	4.90	4.76	8.74	1.00
Using Finger Width=10.25 (mm)	50.2	48.8	89.6	10.2
Measures foot robot implementation (mm)	50	58	100	10.2
Error (absolute and [%])	0.2 [0.4%]	10.8 [18%]	10.4 [10%]	0 [0%]

Table 3.1: Comparison measures

Chapter 4

Experimental results

The last main section of this project, is related to validate the design methodology and the mechanical design itself (i.e. proof of the technology used). The basic idea behind the validation is to replicate the kinematics of an animal leg with a robotic leg featuring the implemented foot while respecting the scaling laws. Kinematics were measured by using a motion capture system and ground reaction forces were measured using force plates. The results will be compared with animal data to examine the validity of the design. The first section of this chapter is devoted to explain the experimental setup, followed by a section with the experiment details. The results and discussion will be provided at the end of the chapter.

4.1 Setup

In figure 4.1, the montage used in the experimental setup is shown. It consist in a robotic leg of two degrees of freedom (2 - DoF) that allows planar robot kinematics to achieve desired position and orientation of the end effector. In this case, the end effector was implemented as the tested foot. Two Dynamixel MX-106R servomotors were employed in this montage. The robotic leg hangs from a horizontal bar that features one horizontal slider. The purposes of this bar are first to constrain the vertical motion of the leg once the end effector is in contact with the ground and second, to provide by means of the slider a horizontal motion that simulates the forward displacement of the sprawling posture robot relative to the static ground contact of the foot. The montage is such that once the foot is lifted a weight connected to the horizontal slider by a rope that passes through a pulley, pulls the leg structure back to the home position (by gravity), in order to repeat the experiment several times without human intervention.

To complement the experimental setup, the mentioned montage, was set along with the Motion Capture system (Optitrack) and the Force plates (Type 9260AA3, Kistler, 2011). In Fig. 4.2 the whole setup can be observed. The markers for the MoCap are selected in a way that all moving parts (i.e. limb and joints) of the leg and foot are tracked sufficiently. This includes the leg upper and lower parts, the ankle, the tarsus, each finger and the finger tips. In the same image, the placement of the force plates underneath the foot is shown, to capture the ground reaction forces (GRF). Extra wood blocks were used to ensure better grip of the foot in contact with the force plates as well as the correct height of the contact point.

Figure 4.1: Experimental montage that comprehends a robotic 2 DoF leg and a supporting structure.

4.2 Experiment

Using the setup mentioned in the previous section (Fig. 4.2), single strides of the leg featuring the implemented foot were tested. A software application was coded. It allowed the control of the three motors (2 for the leg and 1 for the foot actuation). The program consisted in three main functions. The first function was in charge of teaching the robot leg the motion trajectories that it should follow afterwards. This movement is read directly from the internal leg motor encoders and saved in a .txt file (i.e. the position of the motors in time are saved). The second function consisted in generating a sequence of positions for the motor that drives the foot (i.e. pull the internal wires). Interestingly, a simple function was sufficient, as it consisted in moving the motor from 0° to 300° in three steps and then from 300° to 0°. The third function consisted in the integration of first and second functions and execute by playback, the motion of the whole robot's structure.

In order to synchronize the playback data of the taught motion and the actuation of the foot a percentage of the stride time was defined to trigger the foot motor rotation. It was done by selecting a percentage of the stride time. In the first 20% of stride the foot was in extended position (i.e. not generating traction or in home position), from 20-40% it starts generating traction by pulling the rope but with small force value, then from 40-70% there is a complete contraction of the foot (i.e. generate full bending of the fingers) and finally from 70-100% the foot returns to the extended position. The mentioned percentages of foot motor actuation are intended to follow the stride stages, specifically the stance phase from 20-70%.

Once a full stride motion was taught (i.e. movement that the human operator considered a good one compared with animal kinematic data available), the stride was tested in the setup shown in Fig. 4.2. With the MoCap system, kinematic information was measured, and with the force plates, the force applied to the ground was obtained. Two experiments were considered by changing the frequencies of the stride. This was done by replaying the recorded taught data with

Figure 4.2: Setup, using the MoCap and the force plate

different time scales. This is, sending data with different time delays. These two experiments attempt to cover a fairly wide range in the speeds of the stride in order to match lower and upper admissible boundaries of speed according to the scaling laws of the real animal.

4.3 Results and comparisons

4.3.1 Ground Reaction Forces

Experiments as mentioned in the previous section were carried out each one in 10 runs for each speed (i.e. 10 times using a delay of 5 ms in the motor position data sent, called upper speed bound and 10 times for a delay of 10 ms, called lower speed bound). Then, data averages of the experiments were considered. Final results can be seen in Fig. 4.3a. These experiments capture only the gait stance phase, i.e. the data from 500 to 2000 ms for upper speed and 400 to 3200 ms for lower speed.

In Fig. 4.3b, GRFs of the species used in the design and implementation of the foot (Tiger Salamander Ambystoma tigrinum) [32] is provided, however, using a percentage of the stance phase instead of the whole stride as in Fig. 4.3a. It is clear that there is no GRF data for the swing phase as the foot is not touching the ground. However, We decided to include the whole stride length in Fig. 4.3a to visualize all the possible interactions with the ground.

In Fig. 4.3a, for the upper speed routine (red lines), the foot reaches up to 7 N in the Z axis (i.e. Normal force). When the speed decreases to the lower speed, the normal force exerted by the robot's foot increases up to 12 N (blue lines in Fig. 4.3a). For the animal data in Fig. 4.3b, the maximum normal force is 0.4 times its body weight. Differences in absolute values are expected due to factors like the scale, remember from table 3.1, the foot was scaled 10.2 times the real one. The total force scaled up from animal to robot, depends on characteristics like the Froude number, which involves the speed of motion and the gravity. As the purpose of this project was to provide a design methodology for a foot and then implement and test it, the analysis of the correct speed scaling as well as the expected force scaling is out of the scope of this project. However this opens a possible topic to study in the future that will enhance the validity of our

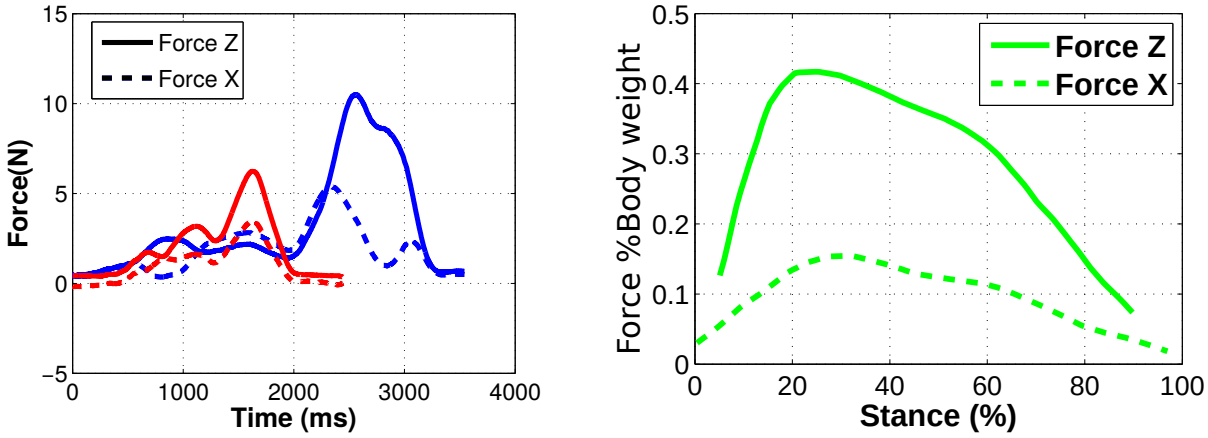

(a) (b)

Figure 4.3: Comparisons between robot and animal GRF. (a) Average GRF results for one stride measured from experiments. Upper speed (red) and Lower speed (blue). (b) Animal data [34].

design. For these reasons, We tried to provide upper and lower speeds and then, the analysis will be more qualitative with respect to the animal data.

Animal data of normal forces during the stance phase (Fig. 4.3b) has a smooth curve. It presents a peak (with the global maximum) in the first 20% of the stance period, then it decreases smoothly. In the robot's data, for example at lower speed, Fig. 4.3a shows a curve (blue line) with two small peaks before the main one. The reasons for the peaks are due to the instants of time when the foot motor was actuated to provide closure to the foot (i.e. increase the stiffness). If the main peak can be considered as the main part of the standing phase, the similarities with the animal data are remarkable. Qualitatively speaking, both forces increase rapidly, sustain a small plateau with an extra peak (maybe due to the finger peeling) and then decrease. The upper speed selected (red in Fig. 4.3a), on the other hand, shows not much detailed information but still presents a smooth increment of the force and the effect of both, the increment of stiffness in the fingers as well as the finger peeling off the ground.

As shown, the normal force decreases as the speed is increased. We hypothesize that as the foot keeps longer time contact with the ground, the normal force registered by the forces plates is higher as it is slowly reduced and converted to forward thrust (this is due to the experimental montage used and its vertical constraint). Nevertheless, further experiments should be done to confirm this hypothesis. Likewise, A way to reduce the differences between the results obtained by the robot and the animal data, is to start the stance phase by generating the maximum force possible (i.e. force to generate traction on the foot). It could be done by applying a weight to the robot's foot.

The X axis force (i.e. anteroposterior force), showed as a dashed line in Fig. 4.3a, presents small values compared to the normal force results. In animal data this anteroposterior force is smooth, whereas in the robot experiment the effect of the foot motor actuation to increase the stiffness of fingers is more notorious. The Y axis direction did not show any significant result (i.e. Y axis force had almost zero Newton values during the experiment due to the setup planar constraint), and for that reason was not considered in this report.

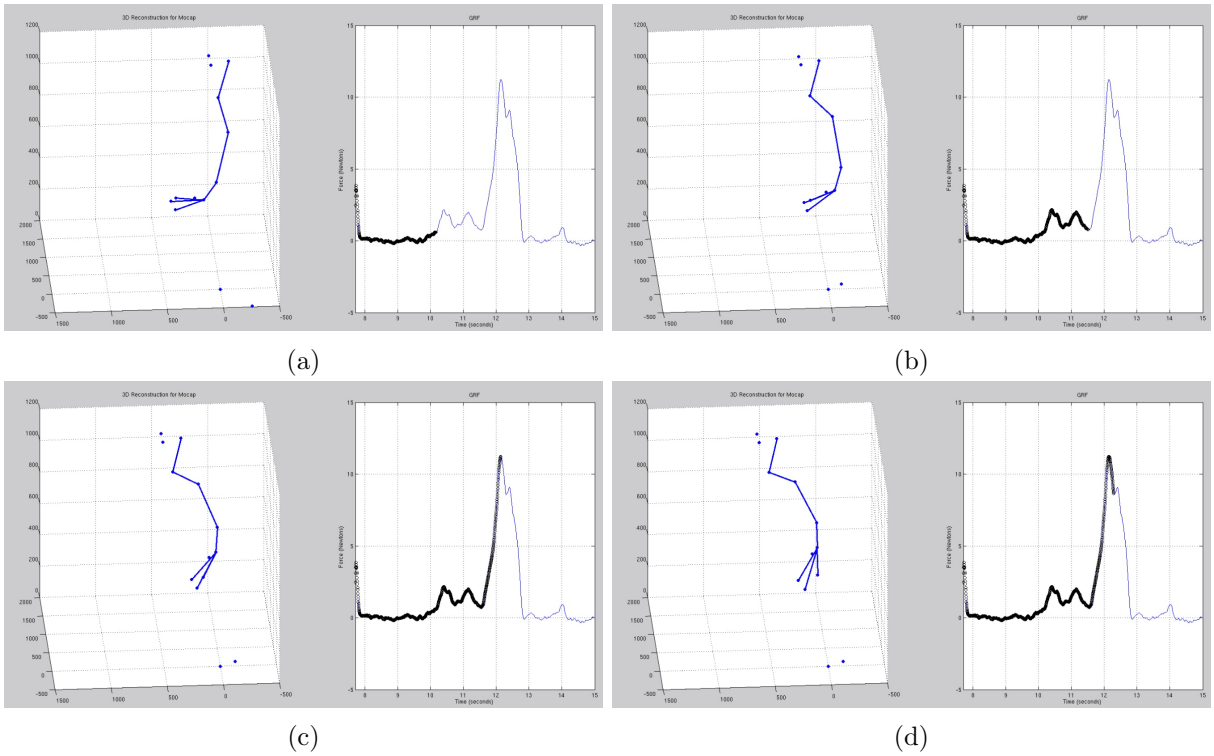

Figure 4.4: MoCap and force plate results at diferent phases of the stride.

4.3.2 Kinematic data synchronization: MoCap and Force Plates

The MoCap system provides kinematic data for the robot's foot while executing the experiments (i.e. X, Y and Z motion data for of each marker as described in the setup section). All data gathered was synchronized with the GRFa, in order to have a better understanding of the performance shown on Fig, 4.3a.

Fig. 4.4 shows the results in a sequential manner, for one selected stride. MoCap data is plotted on the left using blue points to represent the motion capture markers location on the robotic foot and leg (i.e. joints). Blue lines represent the different links that conform such robot. On the right of the same figure, there is the normal force result for the same experiment. The value reached so far by the time of the snapshot is shown in black. In Fig. 4.4, several snapshots of the whole stride are presented.

The first row (a), shows the first snapshot at the exact moment when the stance phase starts i.e. *touch down*. The force plate shows a force value of zero N starting to increase. In the second snapshot (b), the foot is slipping back in a *foot flat* position. In this stage, the foot motor applies a first small amount of force (i.e. force generated by actuate the foot motor synchronized with 20-40% of the standing phase of the recorded in the taught phase). The GRFs show two small peaks, due to the force that the foot starts to generate against the ground once the foot is actuated. In the third snapshot (c), the exact moment when one of the fingers peel off from the ground is shown (i.e. one of the fingers stop contacting with the surface). The GRF shows a fast increase in the force, this is because the finger's foot generate a large amount in normal and thrust forces. The variable compliant nature of the foot starts to play an important role in

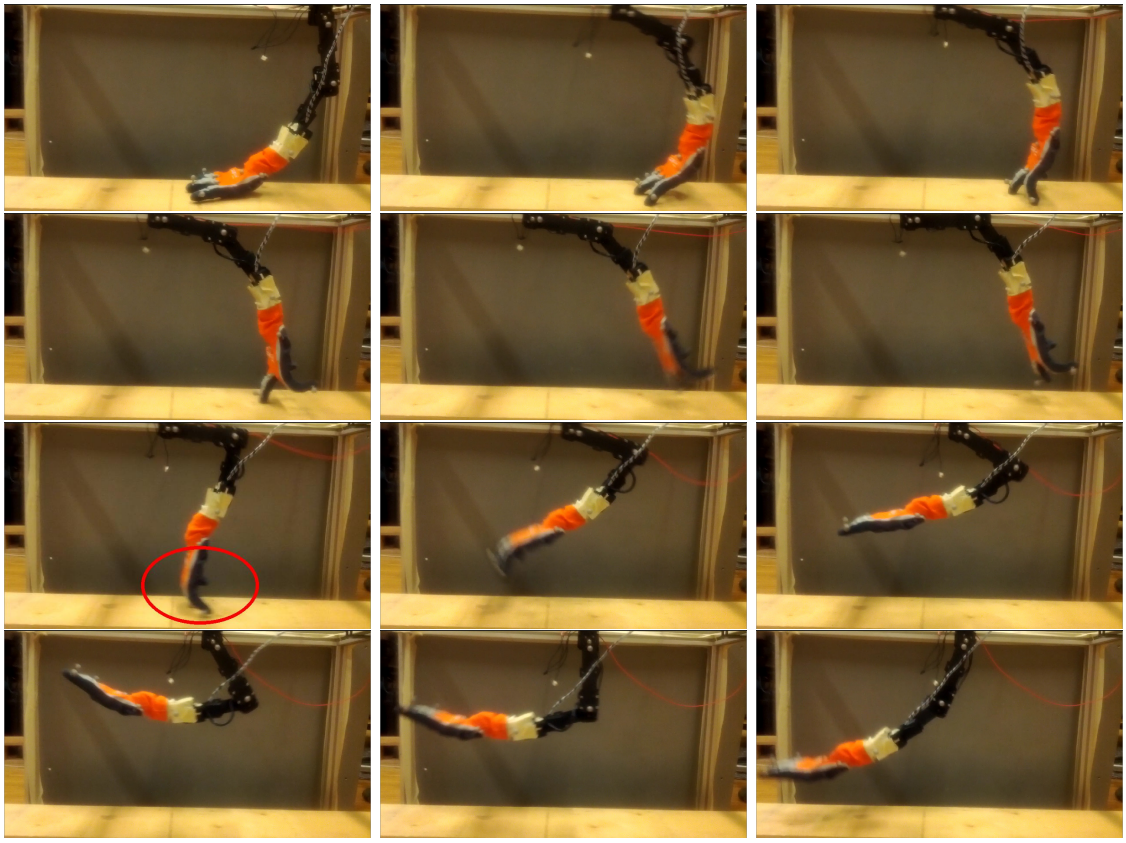

Figure 4.5: Final Sequence. Left to right, top to bottom. Detail of the finger touching the ground in swing phase.

this phase. The foot actuation provided by the motor in the previous stage makes the fingers to start stiffening enough to support the load and produce extra thrust. This is also the beginning of a *push off* phase of the stride.

The foot motor actuates once more, synchronized this time by the 40-70% of the timing in the standing phase. At this point (d), in the fourth row on Fig. 4.4, a second finger peel off the ground. Whereas in the period between the peeling off of first and second fingers the force is reduced, it still presents a high value. This slight reduction of force is due to less fingers exerting force against the ground. At this point, the only supporting finger is loaded with the maximum stiffness of the foot actuation mechanism. At the end of the GRF plot, the normal force become zero, because the third and last finger peel off the ground finishing the *push off* phase of the stride. As there are no contact between the foot and the ground, the GRF reading return to zero N value.

4.3.3 Extra features

One final interesting behavior observed in the experiments, that is worth to keep exploring with this implementation, is the fact that the variable stiffness of the robotic foot is unilateral (i.e. stiff only in one direction and very compliant in the opposite one) . As mention in the previous sections, the fact that the fingers increase their stiffness as the stride progresses, is positive for

the thrust generation. Fig. 4.5 shows one of the experiment sequences executing the whole stride. Just after the peel off of the last finger (i.e. end of the push off phase), the whole foot starts the swing phase to execute the new step. During this swing phase, some of the fingers collide with the ground in some experiments. This is also evident in Fig. 4.4 at the end of the stance phase, where a small peak is shown.

It is true that the finger collides with the ground creating the small peak in the swing phase. However, as the finger is stiff in the opposite direction (i.e. the direction of the traction) it is very compliant in the swing direction. This feature in the foot allows it to collide with several objects during the swing phase (rocks, debris and unevenness in the terrain) which improves the robustness of the whole stride. This is worth to be studied in depth, as in overall this behavior will increase the robustness of any platform that uses this kind of robotic foot. This is one of the main contributions of this project.

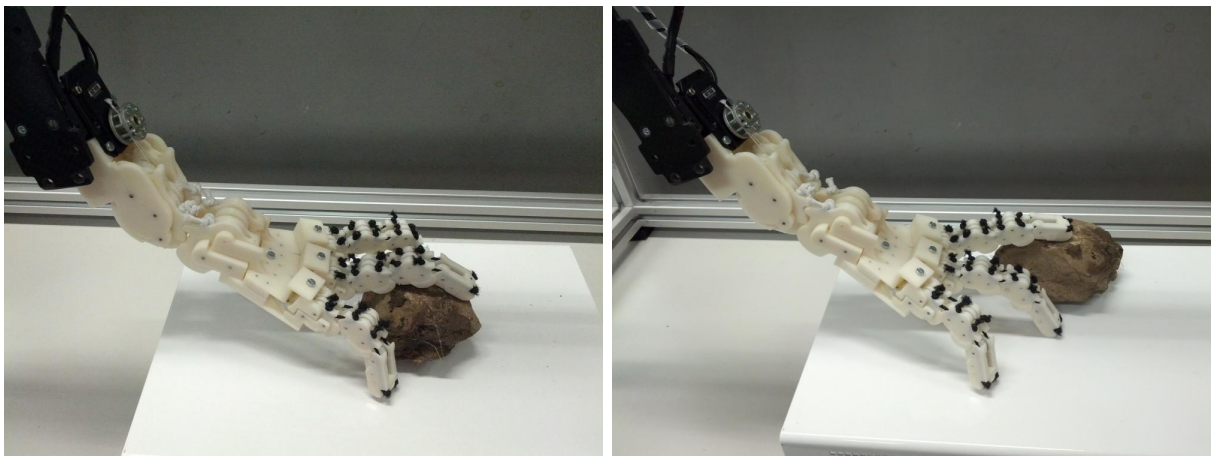

Figure 4.6: Left, two fingers on a rock while the third one adapts to the floor. Right, the same experiment but using only one finger on the rock.

Finally, as seen in Fig. 4.6, another interesting capability of the proposed design is the natural adaptability to the terrain. In the figure, a rock of comparable size was used to prove that as the fingers close on top of this rock, the overall variable stiffness behavior of the mechanism makes it adaptable to an abrupt change in the terrain without compromising the vertical stability. Two fingers lay on top of the rock while the tension of the internal wire is applied. The other finger simply adapt itself to the terrain to provide full vertical support. Likewise, if only one finger lies on the rock, the other two fingers do the respective job by adapting themselves to the terrain keeping the leg vertical, thus providing normal forces without apparent loss of stability.

Chapter 5

Conclusion

As mentioned at the beginning of this report, We hypothesize that fingers and the whole foot structure are important for walking gaits in sprawling posture robots, especially for aquatic stepping gaits, as some recent experiments using Pleurobot indicate a thrust generation due to the finger push off the ground.

The evidence reported in this project, supports the previous hypothesis in the sense that experiments carried out with the proposed foot robot mechanism were sufficient to describe when and how each of the fingers action during the whole stride, contributes to the generation of normal and anteroposterior forces. The stance phase can be now defined from start to end, by the use of the foot and its readings of GRFs, instead of simply looking at the kinematics of the leg solely. In other words, the foot design, provides richer understanding of the locomotion mechanisms while at the same time, simplifying the leg kinematics to only provide placement instead of ground support, as currently robots like Pleurobot do.

Important features like terrain adaptability and simultaneous high resilience to hit obstacles without affecting the stance and swing phases of the stride were observed during the experiments carried out in this project. These are topics worth of further research using the proposed foot design. There is potential in the use of such mechanisms for real field tasks in search and rescue activities. However, further refinements and more experimental data must be provided to ensure the benefits of such a solution.

What is more important, all these presented features related to the final implementation of the robotic foot mechanism, came from a systematic design methodology which is bio-inspired. A contribution so far was on the classification of morphologies and the extraction of simple parameters that allow the design of different feet for different sprawling animals in a generic way. The top-down approach in animal taxonomy allows the user of the methodology to simply locate the biological characteristics like sprawling posture and undulatory spine. Further comparisons between selected species via biomechanical design parameters, allow to reduce the search inside clusters in which the selected species is grouped. Then, the extraction of skeletal foot data and mechanical parameter for the design is straightforward. This is in order to provide the closest biomechanical data that serves as a basis for the final robotic implementation, considering: the technology used for the implementation, its size, the dynamic scaling, and the degree of complexity (or degree of detail) required.

Beyond this design still remain interesting open questions like how to program the adequate foot actuation according to the motion of the whole leg and even more, according to the terrain. In the proposed implementation here, we attempt to create an actuation scheme by steps, triggered

by the percentage of completion of the stance phase. However, as the actuation can be done continuously, the desired trajectory of the foot motor can be modulated in a way that it follows a desired trajectory that maximizes the traction or the support capabilities of the foot. Moreover, this desired trajectory can be optimized in order to adapt the foot interaction with the ground accordingly to the gait scheme, the terrain structure and sensory feedback. In a gaze to the future, this is also a possible first approach for designing a more complex foot with controllable compliant behavior for humanoid robots and human prosthesis as well.

The results of this project were merely quantified to validate the design and to provide a tool for the lab for both, designing generic feet as well as to examine their behavior prior to implementing it in a real robot. For this reason, there is still a lot of work to be done in this area, in the biological classification and extraction of features for foot design as well as their implementation and validation. Nevertheless, We hope this report will create a useful precedent for future work in the EPFL's Biorobotics Lab.

Bibliography

[1] A. J. Ijspeert, A. Crespi, D. Ryczko, and J.-M. Cabelguen, "From swimming to walking with a salamander robot driven by a spinal cord model," *Science*, vol. 315, no. 5817, pp. 1416–1420, 2007.

[2] A. Crespi, K. Karakasiliotis, A. Guignard, and A. Ijspeert, "Salamandra robotica ii: An amphibious robot to study salamander-like swimming and walking gaits," *Robotics, IEEE Transactions on*, vol. 29, pp. 308–320, April 2013.

[3] S. M. Reilly and J. A. Elias, "Locomotion in Alligator mississippiensis: kinematic effects of speed and posture and their relevance to the sprawling-to-erect paradigm," *The Journal of experimental biology*, vol. 201, no. 18, pp. 2559–2574, 1998.

[4] "Dwarf Crocodile." `http://a-z-animals.com/animals/dwarf-crocodile/`. Accessed: 2015-06-03.

[5] D. J. Irschick and B. C. Jayne, "Comparative three-dimensional kinematics of the hindlimb for high-speed bipedal and quadrupedal locomotion of lizards," *Journal of Experimental Biology*, vol. 202, no. 9, pp. 1047–1065, 1999.

[6] C. L. Fieler and B. C. Jayne, "Effects of speed on the hindlimb kinematics of the lizard Dipsosaurus dorsalis," *The Journal of experimental biology*, vol. 201, no. 4, pp. 609–622, 1998.

[7] C. J. Clemente, P. C. Withers, and G. Thompson, "Optimal body size with respect to maximal speed for the yellow-spotted monitor lizard (Varanus panoptes; Varanidae)," *Physiological and Biochemical Zoology*, vol. 85, no. 3, pp. 265–273, 2012.

[8] "Japanese Giant Salamander." `http://www.acecoinage.com/japanesegiantsalamander.html`, Accessed: 2015-06-03.

[9] M. Ashley-Ross, "Hindlimb kinematics during terrestrial locomotion in a salamander (Dicamptodon tenebrosus)," *The Journal of experimental biology*, vol. 193, no. 1, pp. 255–283, 1994.

[10] M. Ashley-Ross, "Metamorphic and speed effects on hindlimb kinematics during terrestrial locomotion in the salamander Dicamptodon tenebrosus," *The Journal of experimental biology*, vol. 193, no. 1, pp. 285–305, 1994.

[11] S. Chevallier, M. Landry, F. Nagy, and J.-M. Cabelguen, "Recovery of bimodal locomotion in the spinal-transected salamander, Pleurodeles waltlii," *European Journal of Neuroscience*, vol. 20, no. 8, pp. 1995–2007, 2004.

[12] K. M. Sheffield and R. W. Blob, "Loading mechanics of the femur in tiger salamanders (Ambystoma tigrinum) during terrestrial locomotion," *The Journal of experimental biology*, vol. 214, no. 15, pp. 2603–2615, 2011.

[13] M. T. Rodrigues, M. Teixeira-Jr, F. Dal Vechio, R. C. Amaro, C. Nisa, A. C. Guerrero, R. Damasceno, J. G. Roscito, P. M. S. Nunes, and R. S. Recoder, "Rediscovery of the Earless Microteiid Lizard Anotosaura collaris Amaral, 1933 (Squamata: Gymnophthalmidae): A redescription complemented by osteological, hemipenial, molecular, karyological, physiological and ecological data," *Zootaxa*, vol. 3731, no. 3, pp. 345–370, 2013.

[14] P. Senter, "Vestigial Structures Exist Even Within the Creationist Paradigm," Tech. Rep. 4, July 2010.

[15] D. B. Wake and N. Shubin, "Limb development in the pacific giant salamanders, Dicamptodon (Amphibia, Caudata, Dicamptodontidae)," *Canadian Journal of Zoology*, vol. 76, no. 11, pp. 2058–2066, 1998.

[16] S. H. Reynolds, *The vertebrate skeleton*. CUP Archive, 2013.

[17] J. Savage, "Studies on the lizard family Xantusiidae IV. the genera ," Oct. 1963.

[18] "Digital Morphology." `http://http://www.digimorph.org`, Accessed: 2015-06-05.

[19] "Green iguana." `http://www.lbah.com/word/wp-content/uploads/2011/12/IggieOVH-Rad.jpg`, Accessed: 2015-06-05.

[20] "Gravid Iguana X-rays." `http://www.herpcenter.com/reptile-articles/gravid-iguana-xrays/`, Accessed: 2015-06-05.

[21] "Articulated Komodo Dragon Skeleton." `https://boneclones.com/product/articulated-komodo-dragon-skeleton`, Accessed: 2015-06-05.

[22] Schachner Emma R., Cieri Robert L., Butler James P., and Farmer C. G., "Unidirectional pulmonary airflow patterns in the savannah monitor lizard," *Nature*, vol. 506, pp. 367–370, feb 2014.

[23] "Monitor Lizard." `https://tsjok45.files.wordpress.com/2012/10/monitors.jpg`, Accessed: 2015-06-05.

[24] "Accidental Land Animals." `https://http://www.geol.umd.edu/~jmerck/geol431/lectures/10stegocephali.html`.

[25] "Japan Salamander." `https://http://4.bp.blogspot.com/-0ggBqgvWDso/UmPNFg1CW1I/AAAAAAAAIFg/WK\_gXHfTHu8/s1600/japansalamander.jpg`.

[26] "Hellberg." `https://http://zoology57.rssing.com/chan-11598120/all\_p19.html`.

[27] "File:Cryptobranchus alleganiensis 2.jpg." `http://commons.wikimedia.org/wiki/File:Cryptobranchus\_alleganiensis\_2.jpg`.

[28] D. B. Wake and N. Shubin, "Limb development in the pacific giant salamanders, Dicamptodon (Amphibia, Caudata, Dicamptodontidae)," *Canadian Journal of Zoology*, vol. 76, no. 11, pp. 2058–2066, 1998.

[29] A. Ivanovic, N. Tomaševic, G. Dzukic, and M. L. Kalezic, "Evolutionary diversification of the limb skeleton in crested newts (Triturus cristatus superspecies, Caudata, Salamandridae)," in *Annales Zoologici Fennici*, vol. 45, pp. 527–535, BioOne, 2008.

[30] "Alligator Skeleton." `https:/http://savalli.us/BIO370/Anatomy/5.AlligatorSkeleton.html`.

[31] M. SIDNEY H. REYNOLDS, *THE VERTEBRATE SKELETON.* at the university press. ed., 1897.

[32] G. B. Müller and P. Alberch, "Ontogeny of the limb skeleton in Alligator mississippiensis: developmental invariance and change in the evolution of archosaur limbs," *Journal of Morphology*, vol. 203, no. 2, pp. 151–164, 1990.

[33] M. A. Ashley, S. M. Reilly, and G. V. Lauder, "Ontogenetic scaling of hindlimb muscles across metamorphosis in the tiger salamander, Ambystoma tigrinum," *Copeia*, pp. 767–776, 1991.

[34] S. M. Kawano and R. W. Blob, "Propulsive forces of mudskipper fins and salamander limbs during terrestrial locomotion: implications for the invasion of land," *Integrative and comparative biology*, p. ict051, 2013.

[35] S. M. Kawano and R. W. Blob, "Propulsive forces of mudskipper fins and salamander limbs during terrestrial locomotion: Implications for the invasion of land," *Integrative and Comparative Biology*, 2013.

[36] R. Safai-Naeeni, "Bioinspired leg design for a salamander robot." June 2012.

[37] P. Schwizer, "Bio-inspired foot design for a salamander robot." Jan. 2014.

[38] K. KARAKASILIOTIS, *Legged locomotion with spinal undulations.* PhD thesis, Jan. 2013.

[39] B. M. Hillberry and A. S. Hall Jr, "Rolling contact joint," Jan. 13 1976. US Patent 3,932,045.

[40] M. G. Catalano, G. Grioli, E. Farnioli, A. Serio, C. Piazza, and A. Bicchi, "Adaptive synergies for the design and control of the Pisa/IIT SoftHand," *The International Journal of Robotics Research*, vol. 33, no. 5, pp. 768–782, 2014.